Bioinspired, Ultra-Light and Sandwich structured MXene-AgNWs/cellulose nanofiber porous film for excellent electromagnetic interference shielding with Joule Heating Performance

Fang Ren
Xi'an University of Technology
Jiale Zhang
Xi'an University of Technology
Tong Wu
Xi'an University of Technology
Fudong Zhang
Xi'an Airborne Electromagnetic Technology Co., Ltd
Zhengzheng Guo
Xi'an University of Technology
Yanling Jin
Xi'an University of Technology
Penggang Ren (rengpg@126.com)
Xi'an University of Technology

Research Article

Keywords: MXene, AgNWs, Cellulose nanofiber (CNF), Sandwich-structured porous film, Electromagnetic interference (EMI) shielding, Joule heating performance

Posted Date: July 10th, 2023

DOI: https://doi.org/10.21203/rs.3.rs-3124085/v1

Additional Declarations: No competing interests reported.

Version of Record: A version of this preprint was published at Cellulose on January 31st, 2024. See the published version at https://doi.org/10.1007/s10570-024-05736-9.

Bioinspired, Ultra-Light and Sandwich structured MXene-AgNWs/cellulose nanofiber porous film for excellent electromagnetic interference shielding with Joule Heating Performance

Fang Ren[a,b,*], Jiale Zhang[a], Tong Wu[a], Fudong Zhang[c], Zhengzheng Guo[a], Yanling Jin[a], Penggang Ren[a,b,*]

a. The Faculty of Printing, Packaging Engineering and Digital Media Technology, Xi'an University of Technology, Xi'an Shaanxi 710048, People's Republic of China

b. School of Materials Science and Engineering, Xi'an University of Technology, Xi'an Shaanxi 710048, People's Republic of China

c. Lightning and Electromagnetic Environmental Laboratory, Xi'an Airborne Electromagnetic Technology Co., Ltd, Xi'an Shaanxi 710077, People's Republic of China

**Corresponding Author: renfang0824@163.com; rengpg@126.com*

Abstract: With the rapid development and popularization of intelligent, portable, and wearable flexible electronic devices, urgently required a new generation electromagnetic interference (EMI) shielding materials to manage the increasing serious radiation pollution. In this work, ultrathin, lightweight, and flexible porous films with reasonable strength were fabricated via vacuum filtered the cellulose nanofiber (CNF) dispersion on both sides of the MXene-AgNWs film and followed by a freeze-drying process. The prepared porous composite film presents to be a typical sandwich-structured with dense in surface and porous inside. This novel and unique structure endows the sandwich-structured porous film with greatly improved EMI performance to 67.5 from 40 dB, enhanced absorption coefficient from 0.1 to 0.4, and satisfactory mechanical properties compared to the conventional sandwich-structured films. Furthermore, the prepared films present the remarkable low-voltage-driven Joule heating performance. Therefore, ultrathin, lightweight,

flexible, and versatile properties CNF-MXene-AgNWs composite porous film with an excellent EMI-shielding performance is hold great potential in the fields of aerospace, portable and wearable electronics.

Keywords: MXene, AgNWs, Cellulose nanofiber (CNF), Sandwich-structured porous film, Electromagnetic interference (EMI) shielding, Joule heating performance

Introduction

The rapid development of telecommunication technology and wearable electronic devices has made electromagnetic radiation pollution problems, seriously affecting the normal operation of adjacent equipment and even human health (Guo, Ren, Lu, et al., 2022; Iqbal, Shahzad, et al., 2020; J. Liu et al., 2022; J. Wang, Ma, Zhou, Du, & Teng, 2022; Wei et al., 2020; Y. Zhang, Ruan, & Gu, 2021). Thus, it is very necessary to reduce the intensity of electromagnetic radiation to an acceptable range. Electromagnetic interference (EMI)shielding materials are capable of solving electromagnetic pollution (Guo et al., 2023; Guo, Ren, Wang, et al., 2022; Y. Zhang & Gu, 2022). Very recently, MXene, as newly emerged two-dimensional transition metal carbide/nitride, presents exceptional metal-like conductivity, which is widely exploited in the field of electromagnetic shielding (M.-S. Cao et al., 2019; Iqbal, Sambyal, & Koo, 2020; H. Liu et al., 2022; Oliveira & Gusmao, 2020; Z. Wang, Cheng, Fang, Hou, & Xie, 2020; Yun et al., 2020). For example, Gogotsi and his co-workers firstly fabricated a free-standing Ti_3C_2Tx-based film (45 μm) with excellent conductivity (4665 S cm^{-1}) and superior EMI shielding effectiveness (SE) of >92 dB (Shahzad et al., 2016). Since the conductivity of pure MXene film is too high to meet the impedance matching, which is easy to cause a large number of surface reflection. Therefore, it is necessary to improve the attenuation performance of Ti_3C_2Tx MXene composite film for electromagnetic waves by carefully designing the morphology through interface engineering.

In order to alleviate the above predicament, more explorations are attempted to optimize the preparation process by foam methods (Deng, Tang, Wu, Zhang, & Yu, 2021; X. Wu et al., 2020; Zhu et al., 2021). After foaming, the composite not only exhibits low density and lightweight by introducing a large number of holes, but also enhances the internal absorption and dissipation efficiency of electromagnetic waves by creating multiple interfaces (Q. Chen, Zhang, Huang, Li, & Yuan, 2022; Z. Chen, Xu, Ma, Ren, & Cheng, 2013; Han et al., 2019). However, the traditional formation strategies of foamed/porous structure, such as freeze-drying, supercritical CO_2 foaming, and the template method, inevitably interrupt the construction of the conductive network by introduced air bubbles and reduce the overall shielding performance (Fan et al., 2020; H.-B. Zhang, Yan, Zheng, He, & Yu, 2011). Thus, to achieve ideal EMI SE, a large thickness is usually needed, which will result in poor flexibility and mechanical strength.

The developed foamed composites with efficient EMI shielding performance in recent years were of ultrathin, light weight, flexible, and high absorption characteristics (Liu et al., 2017; Tang et al., 2022; Y. Zhang, Ruan, Shi, et al., 2021). Zhang et al. successfully prepared $Ti_3C_2T_x$-based graphene porous composite films ($Ti_3C_2T_x$-rGO) by decomposition of NH_4HCO_3 as foaming agent during heat treatment (350 ºC, 2h and hydrogen-argon atmosphere). Due to the synergic effect of the high electrical conductivity and porous structure, the obtained $Ti_3C_2T_x$-rGO with a thickness of 60 μm achieved the maximum value of 59 dB. In addition, Yu and co-workers fabricated lightweight and flexible MXene foams with desirable strength and superior EMI Shielding via the hydrazine-induced foaming process. A greatly enhanced EMI-shielding performance was achieved for the MXene foam (~70 dB) compared to its unfoamed film (~50 dB) because of its favorable porous structure (Liu et al., 2017). Nevertheless, MXene foam are confronted with the issue of poor mechanical properties due to loosing pore structure. Besides, the heating treatment requires harsh conditions and hydrazine-induced foaming process does harm to human health and environment, which limit the large-scale application of the foam (Tang et al., 2022). Therefore, how to realize the rational construction of ultrathin, lightweight, flexible, and high mechanical strength MXene porous film with excellent EMI SE becomes a crucial challenge.

Cellulose nanofibers (CNF) produced from plant-derived renewable resources display outstanding mechanical properties (e.g., Young's modulus up to 250 GPa, intrinsic flexibility, etc.), high aspect ratio, low density, and smooth surface (Lapka et al., 2023). Recently quite a few researchers have chosen CNF as flexible substrate and reinforcing fillers to support MXene (Bai et al., 2022; W.-T. Cao et al., 2018; Yuehu Li, Chen, Liu, Zhang, & Qi, 2021; Wan et al., 2021). For instance, Chen et al used CNFs to fabricate MXene-based composite film, which has great mechanical property (Zhan, Song, Zhou, & Lu, 2019). However, the insulated CNF blocks the electrons transmission between MXene layers, thus, decreasing the EMI performance property. Therefore, it is still a great challenge to fabricate MXene/CNF composites with excellent mechanical strength and EMI shielding property.

Skeleton, one of the hardest tissue of a person or animal, has a complex internal with a honeycomb-like three-dimensional structure and a dense external structure, thus exhibiting high mechanical strength while reducing weight. As exemplified by the case of skeleton, the construction of skeletal structures (sandwich bionic porous structure) can effectively improve the mechanical properties of materials, electromagnetic shielding properties and meet the requirements of light weight. Therefore, in this work, we demonstrate a facile approach to prepare the sandwich bionic porous MXene-AgNWs/CNF by vacuum filtering the CNF dispersion on both sides of the porous MXene-AgNWs film. The outer CNF layers not only endow the composite film with excellent mechanical strength, but effectively improve the oxidation resistance. More importantly, the porous internal structure of MXene-AgNWs greatly enhanced EMI-shielding performance and strong absorption capacity. In addition, the prepared composite porous films present high Joule heating temperature at relatively low applied voltages and rapid Joule heating response. This work provides novel insights for the designing multifunctional EMI shielding materials for aerospace, artificial intelligence, and next-generation flexible wearable electronic devices.

1. Experimental

2.1 Materials

MAX (Ti_3AlC_2 powder, 400 meshes) were bought from Jilin 11 Technology Co., Ltd. Silver nanowires (AgNWs) suspension (10 mg/mL, 20-30 nm in diameter, 10-15 µm in length), was supplied by Zhejiang Kechuang Advanced Materials Co., Ltd. Cellulose nanofiber (CNF) aqueous solution (1 wt%, 0.8-2.0 µm in length) was obtained from Tianjin Woodelf biotechnology Co., Ltd. Lithium fluoride (LiF, ≥ 99.0%, AR) and hydrochloric acid (HCl, 35−37 wt% in H_2O) were provided from Shanghai Macklin Biochemical Co., Ltd., China. All chemicals were used as received without further purification.

2.2 Fabrication of the sandwich bionic MXene-AgNWs/CNF porous film

$Ti_3C_2T_x$ MXene was synthesized according to our previous works (F. Zhang et al., 2022; Zong et al., 2022). As illustrated in Figure 1, the sandwich bionic MXene-AgNWs/CNF porous films were prepared via a controlled vacuum-assisted filtration and freeze-drying methods. Firstly, 12.5 mL of CNF dispersion with a concentration of 2 mg/mL was vacuum filtered (vacuum filtration I) onto the poly(ethersulfone) membrane until the formation of a stable CNF hydrogel. Then, a homogeneous mixed dispersion of 50 mg of $Ti_3C_2T_x$ MXene and AgNWs in different ratios of 10:0, 9:1, 7:3, 5:5, and 3:7, respectively, was stirred ultrasonically and deposited on the above of the CNF hydrogel (vacuum filtration II). Thereafter, 12.5 mL of CNF dispersion with a concentration of 2 mg/mL was deposited on the topmost layer (vacuum filtration III) in the same way. Finally, the obtained sandwich-structured hydrogels were frozen longitudinally under liquid nitrogen until the films were completely frozen and formed, and then the films were vacuum freeze-dried to obtain sandwich bionic MXene-AgNWs/CNF composite porous films. For simplicity, the sandwich bionic MXene-AgNWs/CNF porous films were labeled as CM_XA_YC, where x and y represent the mass ratio of the $Ti_3C_2T_x$ MXene and AgNWs, respectively. The prepared composite film showed a honeycomb-like three-dimensional structure inside, exhibiting lightweight characteristics.

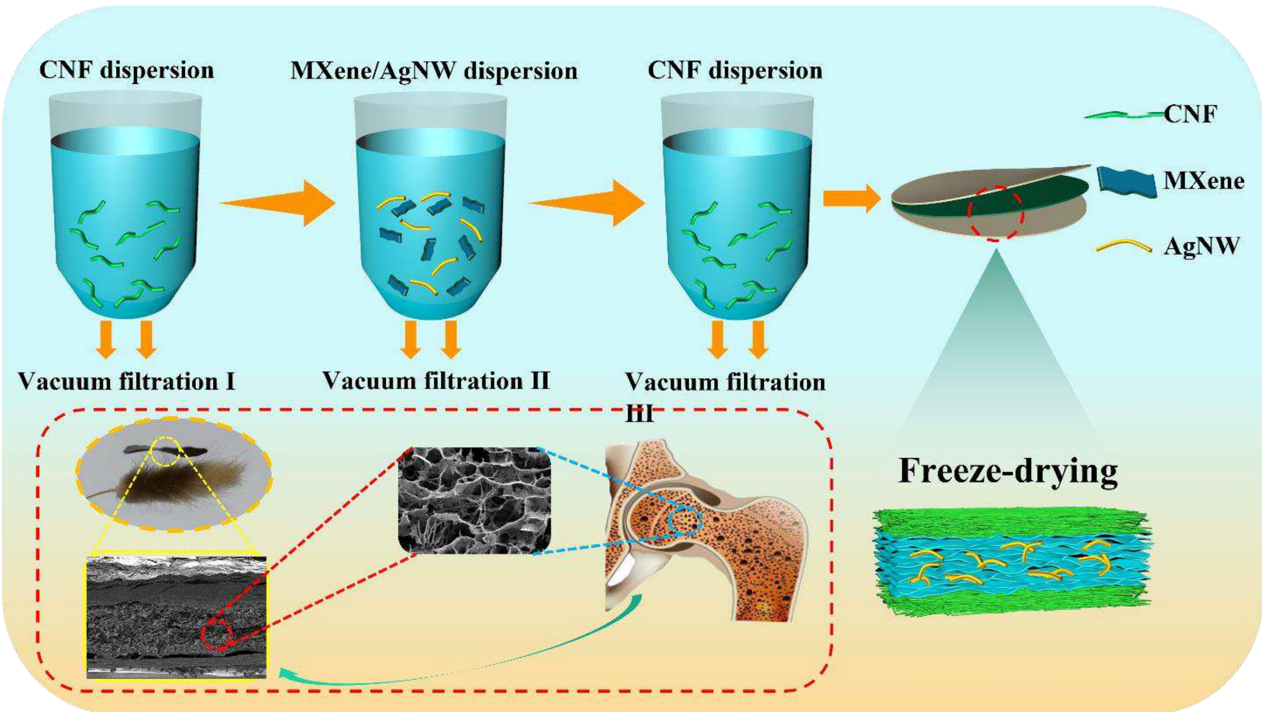

Figure. 1. Schematic diagram of the manufacturing process of laminated bionic composite films.

2.4 Characterization

The structural morphologies and microstructures of the samples were observed by the field scanning electron microscopy (SEM, FEI Inspect-F, Finland) and transmission electron microscopy (TEM, JEM 2100, JEOL). X-ray photoelectron spectra (XPS, XSAM800, Japan) were employed to analyze the surface chemical compositions and chemical bond of Ti_3C_2Tx MXene. The phase compositions of the samples were characterized by X-ray diffraction (XRD, TTRIII, Rigaku, Japan). The resistance of samples was measured by a Keithley electrometer Model 4200-SCS (USA) according to a two-point method. The electrochemical workstation (RST 5200, Suzhou Resitest Electronic) was used to record the voltammetric current signals. The electrical conductivity of the sandwich bionic CNF-MXene/AgNWs composite porous films was calculated as Eq.1:

$$\sigma = L/RA \quad (1)$$

where σ is the electrical conductivity (S cm^{-1}), R is the resistance (Ω), L is the length of the test samples (cm), and A is the cross-sectional area of the measured samples (cm^2). The mechanical tests of samples were performed at RT by a universal testing machine (UTM2103) with a sample rectangle size of 25 × 5 mm^2 and loading rate of 0.5 mm/min. The surface temperature of the composite film was recorded using an infrared thermal imager (Fluke Ti300).

The EMI SE of the as-prepared films was measured by an Agilent N5247A vector network analyzer. All samples were cut into cylindrical shape with the diameter of 13 mm for measurements. The scattering parameters (S_{11} and S_{21}) in the frequency range of 8.2-12.4 GHz were recorded, and the coefficients of reflectance (R), absorption (A) and transmittance (T), EMI SE (SE_T), microwave reflection (SE_R) and microwave absorption (SE_A) were calculated using the following equations:

$$R=|S_{11}|^2, T=|S_{21}|^2 \quad (2)$$

$$A=1-R-T \quad (3)$$

$$SE_R(dB)=-10\log(1-R), SE_A(dB)=-10\log(T/(1-R)) \quad (4)$$

$$SE_T(dB)=SE_R+SE_A+SE_M \quad (5)$$

Where SE_A is the absorption value, SE_A is the reflection value, and SE_M is the microwave multiple internal reflections, which can be negligible when SE_T is higher than10 dB (Abbasi, Antunes, & Ignacio Velasco, 2019; Kim, Lee, Kim, & Lee, 2010). In order to fairly compare the effectiveness of the shielding materials, the density and thickness of the shielding materials are also considered. The related equations were described as:

$$SSE(dB\ cm^3g^{-1})=EMI\ SE/density \quad (6)$$

$$SSE/t(dB\ cm^2g^{-1})=SSE/thickness \quad (7)$$

2. Results and discussion

3.1 Morphology and structure characterization

Figure 2a shows the XRD patterns of $Ti_3C_2T_x$ MXene and Ti_3AlC_2 MAX. After etching, the absence of the main peak (104) located at 39° and the peak (002) shifting from 9.64° to 6.66°, indicate the successful synthesis of MXene (Zhu et al., 2021). The XPS wide-scan spectra of the Ti_3AlC_2 MAX and $Ti_3C_2T_X$ MXene, as well as the high-resolution spectra of Ti 2p, O 1s, F 1s and C 1s are displayed in Fig. 2b−f. Al 2p at around 74 eV for Ti_3AlC_2 MAX disappears completely, indicating the Al layer is selectively etched. The Ti 2p spectrum shows two peaks of Ti $2p_{1/2}$ and Ti $2p_{3/2}$, containing Ti–C (460.2 and 455.1 eV), Ti^{2+} (460.9 and 456.0 eV), Ti^{3+} (462.1 and 457.1 eV) and Ti–O (463.2 and 458.3 eV). The four peaks located at 530.1, 530.6, 532.5, and 533.8 eV, assigned to C–Ti-Ox, C–Ti-OHx, C=O and C-O, are detected in O1s, indicating the existence of oxidized region. The F 1s spectrum exhibits two main peaks (684.8 eV and 686.4 eV), which belong to C-Ti-Fx and Al-Fx, respectively. Five peaks appear in C 1s spectrum: C–Ti-Tx bond at 284.1 and 282.5 eV, C–C bond at 284.8 eV, C–H/C–O bond at 285.6 eV, and C–O/C–O–C bond at 287.0 eV. The morphology and structure of the prepared $Ti_3C_2T_X$ was characterized by SEM and TEM, and the corresponding results are presented in Fig. 2g-i, respectively. The prepared $Ti_3C_2T_X$ exhibits a typical accordion-like microstructure (Fig.2g-h), which further demonstrated that Al layer has been successfully etched. The TEM image of $Ti_3C_2T_X$ MXene dispersion shows clear transparent feature and few-layer 2D nanosheets (shown in Fig.2h).

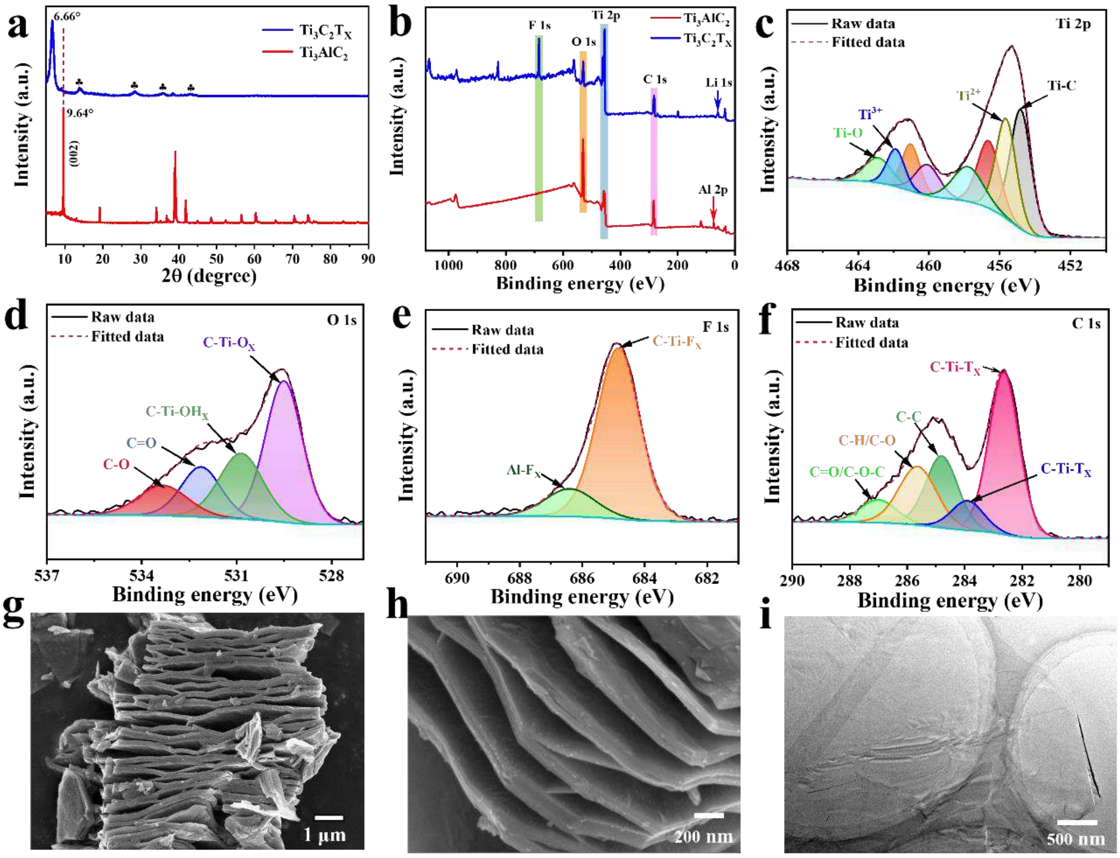

Figure. 2. (a) X-ray diffraction (XRD) patterns and (b) X-rayphotoelectron spectroscopy (XPS) survey spectra of Ti_3AlC_2 MAX and delaminated $Ti_3C_2T_X$ MXene. High resolution XPS spectra of (c) Ti 2p; (d) O 1s; (e) F 1s and (f) C 1s of $Ti_3C_2T_X$ MXene. (g, h) Scanning electron microscopy (SEM) images and (i) Transmission electron microscopy (TEM) image of $Ti_3C_2T_X$ MXene

Figure 3 presents the surface and cross-sectional SEM images of the CM_7A_3C. As shown in Fig. 3a, the composite film exhibits a relatively smooth and dense structure over the entire surface. From the Fig. 3b-f, the CM_7A_3C exhibits obvious morphological difference between outer-layer and core-layer. The cellulose nanofibers tightly interwoven together on both sides of the CM_7A_3C, exhibiting a smooth cross-sectional morphology, while the core-layer of MXene-AgNWs shows a honeycomb-like three-dimensional structure (Fig. 3c-d), which provides the material with lightweight. Note that the MXene sheets are not separated individually, but partially glued to each other to form a continuous cellular structure due to the sublimation of the ice during freeze-drying (Fig.3d). It can be clearly observed in Fig.3e-f that AgNWs are randomly cross-distributed between MXene lamellae as interlayer "linkers" and "hardeners", which are conducive to the formation of a dense multi-channel conductive network. The cross-sectional SEM images of CM_3A_7C are depicted in Fig. S1. As can be seen, a large number of AgNWs interwove with each other, and the internal pores decreased significantly due to the reduction of MXene. In addition, the distribution of each component in CM_7A_3C was investigated by element mapping, and Fig. 3g shows the element selective distribution of Ti, C, and Ag in the composite film. In particular, the distribution of Ti and Ag elements is in perfect agreement with the distribution of the intermediate layer MXene and AgNWs observed in the SEM images, further demonstrating the composite film's layered porous structure.

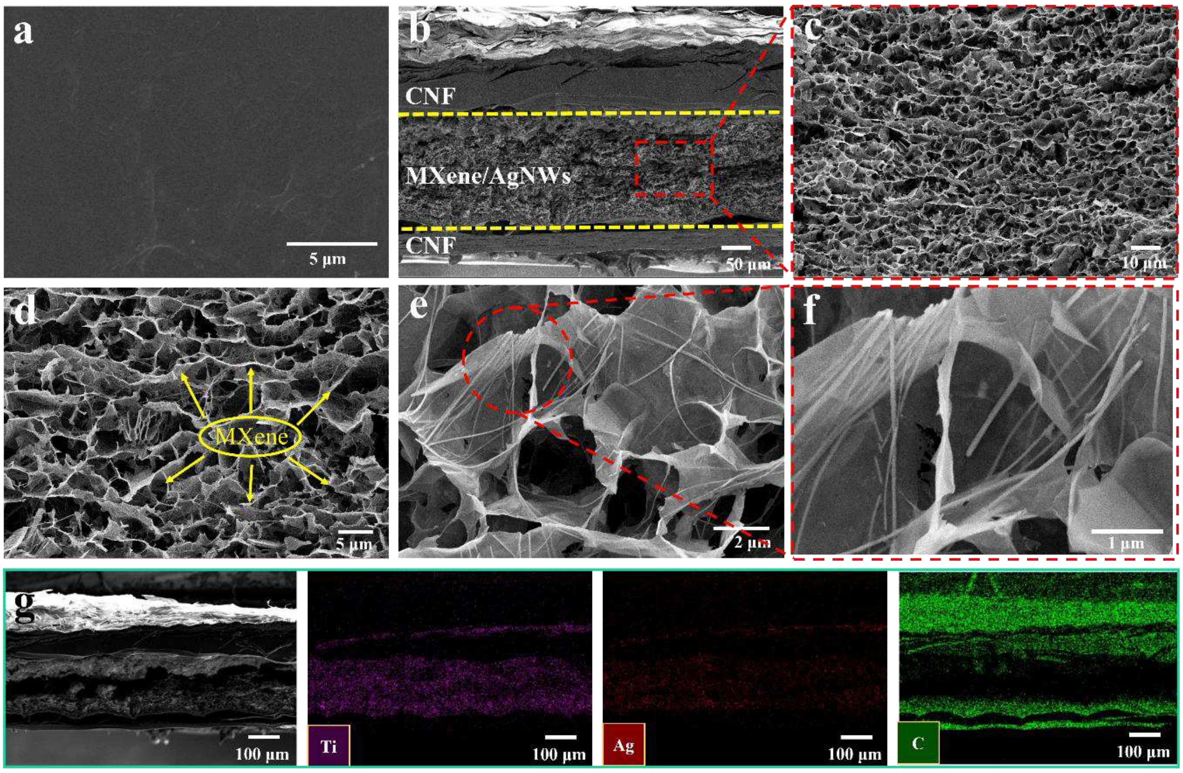

Figure 3. SEM images of the CM_7A_3C (a) surface SEM image, (b-g) Cross-sectional SEM images, and the elemental mapping (g) of the CM_7A_3C sample.

3.2. Electrical and EMI shielding performance of the sandwich bionic MXene-AgNWs/CNF composite porous films

The electrical conductivity (σ) of a material is an important influence on its EMI SE. High electrical conductivity is often conducive to excellent electromagnetic shielding performance (Tan, Gou, Zhang, Ding, & Wang, 2023). The σ of the obtained CM_XA_YC is shown in Fig. 4a. The conductivity of the composite films showed an upward trend, increasing from 1.22 S/cm to 35.09 S/cm as the ratio of MXene and AgNWs changed from 10:0 to 3:7. This is mainly due to the tightly connected conductive network as the content of AgNWs increases. The conductivity evolution was more clearly from the brightness of the LED lamp, which further reflects the change of the σ at different ratios of MXene and AgNWs.

Figures 4b and c display the EMI shielding performance of the sandwich bionic MXene-

AgNWs/CNF porous films in X-band (8.2-12.4 GHz). As expected, the fabricated composite porous films exhibit high EMI SE due to its outstanding electrical conductivity and porous structure. Besides, the EMI SE enhanced dramatically first and then decreased with increasing AgNWs ratios (Fig. 4b). Specifically, the electromagnetic shielding values of the composite films with MXene and AgNWs ratios of 10:0, 9:1, 7:3, 5:5 and 3:7, reached 44.8 dB, 53.6 dB, 67.5 dB, 61.3 dB, and 55.9 dB, respectively. The best electromagnetic shielding performance of the prepared films was achieved at the MXene and AgNWs ratio of 7:3. This phenomenon is due to the perfect porous structure inside the composite film when the MXene/AgNWs ratio is 7:3. The reflection efficiency (SE_R) and absorption efficiency (SE_A) derived from the SE_T are employed to evaluate the EMI shielding mechanism (Fig. 4c). As the ratio of MXene and AgNWs changes, the SE_T and SE_A of the composite porous films exhibit a clear variation. At the same time, SE_A contributes more to EMI SE than SE_R. However, all of the conductive films have SE_R values in excess of 3 dB, manifesting that over 50% of the EMWs are reflected. Thus, SE_R cannot estimate the EMW reflected from the surface of the material due to the impedance mismatch. Based on it, power coefficients such as reflection coefficient (R), absorption coefficient (A) and transmission coefficient (T) are calculated to evaluate the real EMI shielding mode. Fig. 4d-e show the R-A coefficients of all the composite porous films. As illustrated, the R values are always a little bit higher than A values, which implies a reflection-dominated shielding mechanism. Despite this, compared to conventional composite films prepared by vacuum-assisted filtration in which more than 90% of the EMWs are reflected at the surface, the composite porous films prepared in this paper effectively improve the absorption loss of incident EMWs. Furthermore, Fig. S2 plots the power coefficients of the CM_7A_3C at X-band compared with the films with 7:3 ratio of MXene to

AgNWs (named C-F) obtained by the conventional vacuum-assisted filtration method. The A coefficient of CM_7A_3C can reach 0.4, which is much higher than 0.1 for C-F. In summary, the prepared sandwich-structured porous composite film exhibits improved absorption loss of incident electromagnetic waves. Meanwhile, Fig. S2 compares the EMI SE of the sample C-F and CM_7A_3C. As can be seen, CM_7A_3C is substantially improved to 67.5 dB from 40 dB of C-F. In practical application, in order to fairly compare the effectiveness of the shielding materials and eliminate the effect of density and thickness on the electromagnetic shielding performance, the specific shielding performance (SSE) and SSE/t of the CNF-MXene/AgNWs composite porous film is introduced to evaluate and compare with the reported literature. As shown in Figure 4f and table 1, the Mxene-AgNWs/CNF composite films prepared in this paper exhibit excellent SSE/t values, with the highest SSE/t value reaching 10675 dB·cm^2·g^{-1}.

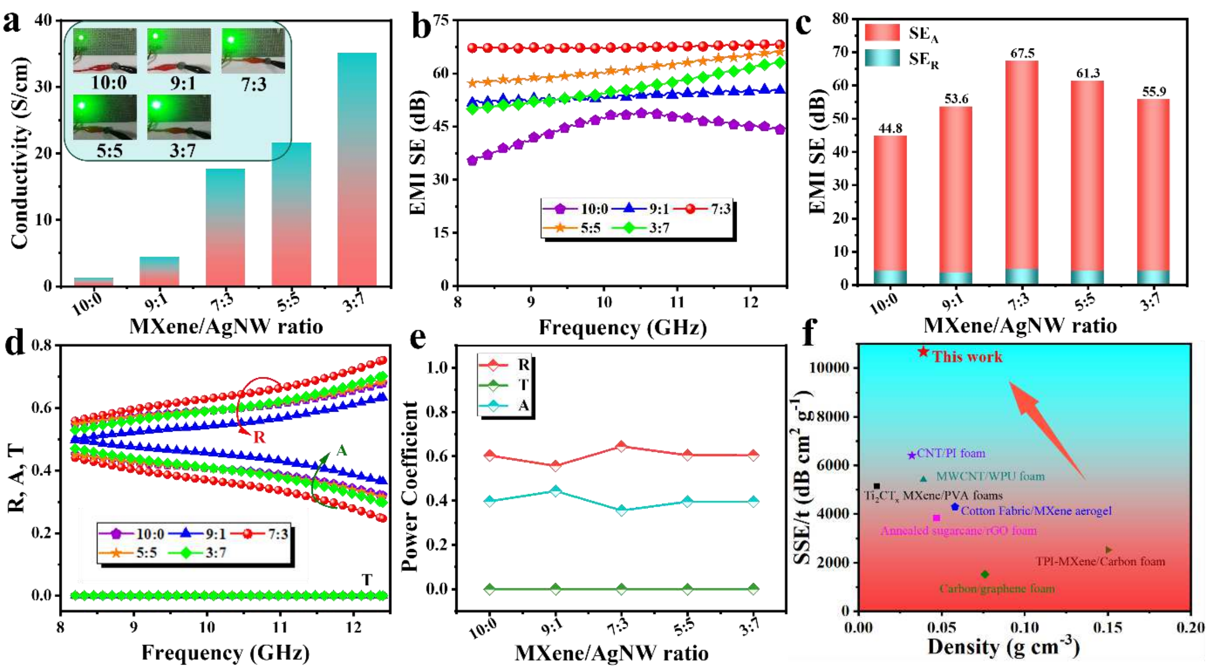

Figure. 4. (a) Conductivity, (b-c) EMI SE and (d-e) Power coefficients composite films with different ratios of MXene and AgNWs (10:0, 9:1, 7:3, 5:5 and 3:7, respectively). (f) Comparison of SSE/t as a function of thickness with previous reports.

Table 1. Comparison of EMI shielding performance of the sandwich bionic Mxene-AgNWs/CNF porous film and other porous materials.

Samples	**EMI SE (dB)**	**Density (g cm^{-3})**	**SSE/t (dB cm^2 g^{-1})**	**Ref.**
TPI-MXene/Carbon foam	44.7	0.15	298	(Jia, Shen, Zhang, & Zheng, 2021)
Graphene/PI aerogel	28.8	0.076	1518	(Yu, Dai, Yuan, Zou, & Liu, 2020)
Carbon/graphene foam	51	0.72	970	(Yang Li et al., 2016)
CNT/PI foam	41.1	0.0321	6402	(Y.-Y. Wang et al., 2020)
Cotton Fabric/MXene aerogel	42.1	0.058	4299	(Zhai et al., 2022)
Annealed sugarcane/rGO foam	53	0.047	3830	(L. Wang, Shi, Zhang, Zhang, & Gu, 2020)
MWCNT/WPU foam	21.1	0.039	5410	(Zeng et al., 2016)
Ti_2CT_x MXene/PVA foam	28	0.0109	5136	(Xu et al., 2019)
MXene/silver nanowire/PU foam	50	0.15	2525	(Cheng et al., 2021)
CNF/Mxene-AgNWs porous film	67.5	0.158	10675	This work

To better elucidate the EMI shielding mechanism, the speculated EMWs transmission path is depicted in Fig.5. When the incident EMWs strike the CNF layers, nearly all of the EMWs can readily enter the porous films due to the good impedance matching. When the incident EMWs reach the porous MXene-AgNWs conductive layer, the EMWs will undergo reflection, absorption, and multiple reflection in porous structured layer. Specifically, as EMWs pass through the MXene-AgNWs porous layer, the sheet-like pores acting as shielding walls, effectively extend the internal electromagnetic wave transmission path, and the multiple internal reflections and scatterings allow the remaining electromagnetic waves to continue to be attenuated by conductive losses. This "absorption-reflection-reabsorption" process continues until the electromagnetic waves are completely depleted.

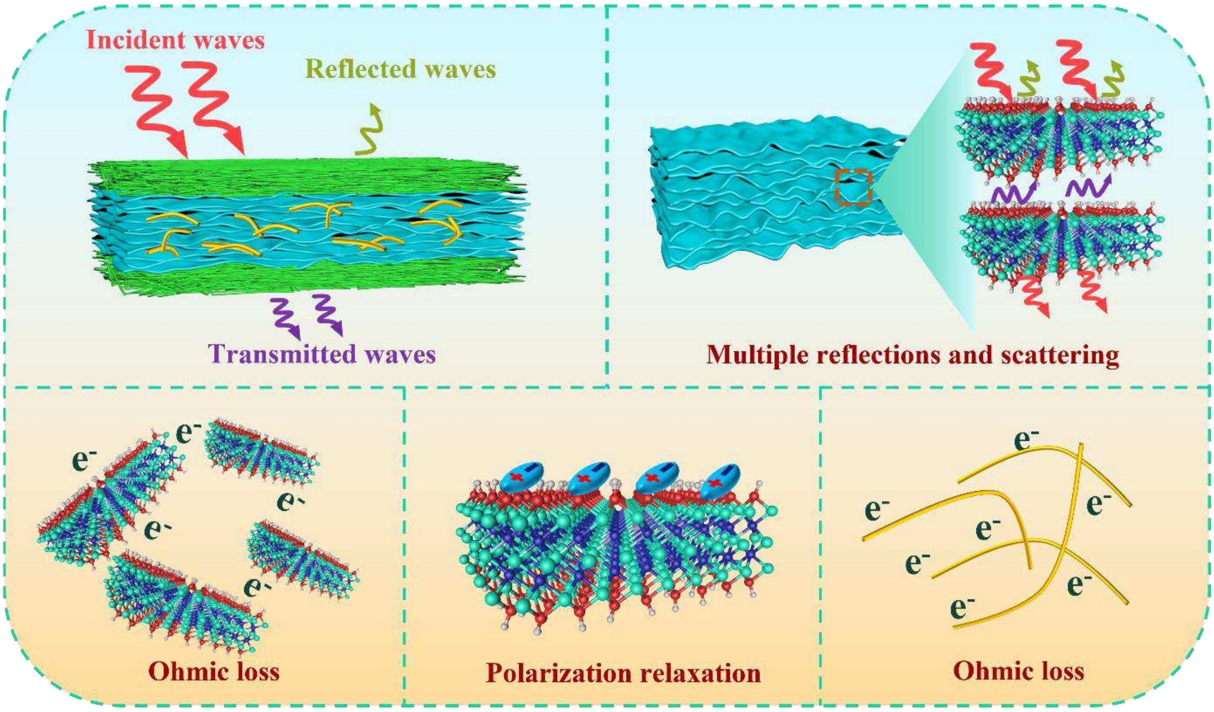

Figure 5. Schematic diagram of electromagnetic wave transmission on a composite CNF-Mxene/AgNWs film with a sandwich bionic structure.

3.3. Mechanical properties of the sandwich bionic MXene-AgNWs/CNF composite porous films

Apart from remarkable EMI shielding property, excellent mechanical property is also an important parameter for the practical application of next-generation EMI shielding materials. Thus, tensile test was used to evaluate the mechanical property of the composite porous films, and the relevant results are shown in Fig. 6a-b. Pure $Ti_3C_2T_x$ MXene films are brittle fracture due to poor interfacial interactions, which makes them unsatisfactory for practical application requirements (Quero & Rosenkranz, 2021). The prepared sandwich bionic CNF/Mxene-AgNWs porous film can improve the mechanical property to the maximum extent because of the presence of bilateral CNF lamellar structures. Figures 6a shows representative stress-strain curves for MXene-AgNWs/CNFporous film. In the range of $Ti_3C_2T_x$ MXene and AgNWs ratios from 10:0 to 3:7, the tensile strength and elongation at break of the sandwich bionic composite porous films reached considerably high levels of 18.2-20.3 MPa and 1.8-2.1% (Figures 6b). Besides, the abundant functional groups of the CNF (seen in Fig.S3) are also beneficial for chemical crosslinking of the MXene, significantly improving mechanical property and oxidation stability (N. Wu et al., 2023) . In order to more clearly illustrate the mechanism of strengthening toughness, the fracture process of MXene-AgNWs/CNF with sandwich structure under tension is depicted in Figure 6c. The fracture mechanism can be elucidated as follows: the MXene-AgNWs layer ruptures firstly due to weak interlayer interactions. Then, the robust CNF layer prevents the initial crack in the rigid but brittle MXene-AgNWs layer from spreading throughout the film. When CNF reaches the ultimate load, the cracks propagate to the interface and spread to the CNF layer in nanoscale "zigzag" crack paths, while micrometer-scale "zigzag" crack paths are formed between the layers.

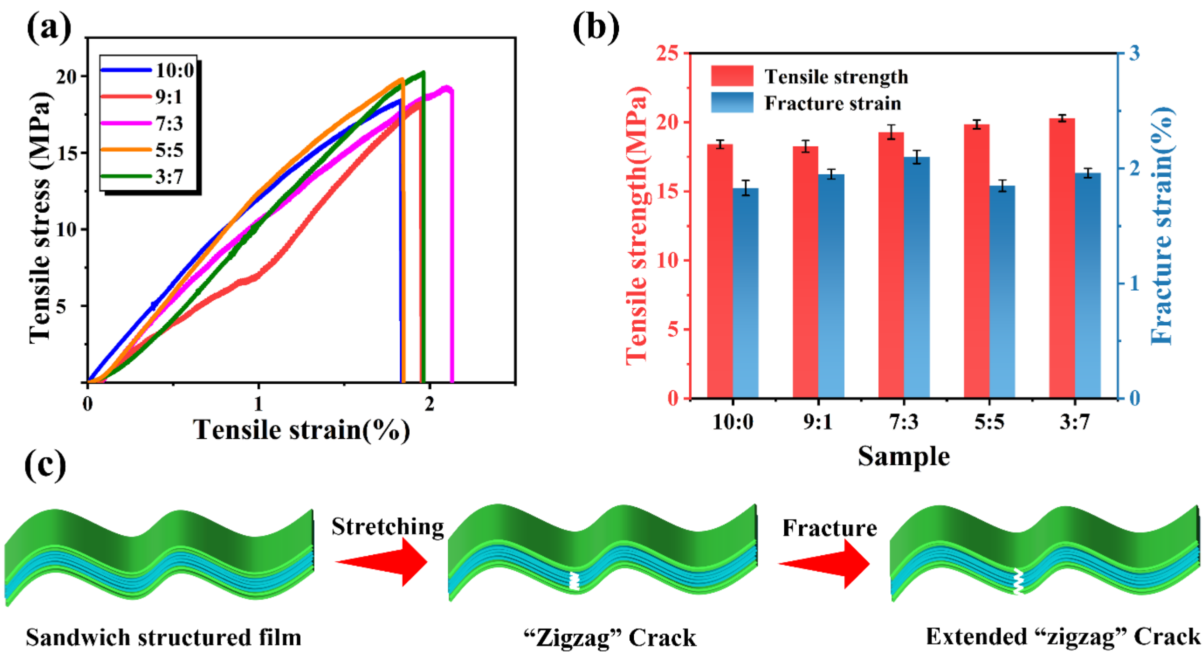

Figure. 6. Mechanical properties of the composite films with MXene and AgNWs ratios of 10:0, 9:1, 7:3, 5:5 and 3:7: (a) Tensile stress-strain curves; (b) Tensile strength and fracture strain; (e) Schematic diagram of the fracture mechanism.

3.3. Joule heating performance

According to Joule's law ($Q=\frac{U^2t}{R}$, where Q, U, R and t are the generated heat, applied voltage, resistance of the material and working time, respectively), the high conductivity confers a satisfactory Joule heat capacity to the prepared MXene-AgNWs/CNT films, ensuring the proper operation of the electrons in the device under extremely cold conditions (Hu et al., 2022; L. Zhang et al., 2022). Figure 7a represents the surface temperature of the prepared MXene-AgNWs/CNT films as heaters recorded by the infrared imager at low applied voltages of 0.5-2.5 V. The surface temperature of all the heaters rapidly reaches a maximum and then remains stable, indicating a state of equilibrium between the photothermally induced and dissipated heat. After the voltage turned off, the temperature drops rapidly to the initial value. Obviously, the greater the voltage applied, the higher the equilibrium temperature. The equilibrium temperature is 44.5 ◦C when the voltage is 0.5 V, and when the applied voltage rises to 1.5 V, it greatly rises to 63.5 ◦C, and further increases to 94.6 °C at the voltage of 2.5 V. After unplugging the voltage, the temperature drops below 30 ◦C within 13 s. In addition, the plateau saturation temperature of the MXene-AgNWs/CNT film was linear to the square of the applied voltage (Figure 7b), in accordance with Joule's law. The strong dependence of the surface temperature on the applied voltage indicates that the prepared composite films have a highly controllable joule heating capacity. The temperature variation of the MXene-AgNWs/CNT film surface when the applied voltage was varied from 0.5 to 2.5 V was further shown by infrared thermal images (see the insets in Fig. 7b). The obtained thermal infrared images show a uniform temperature distribution, which is an important criterion as an electric heater. These results indicate that the prepared MXene-AgNWs/CNT exhibit low trigger voltage and outstanding Joule heating performance, which has potential applications in the field of electric heating clothing and thermal therapy.

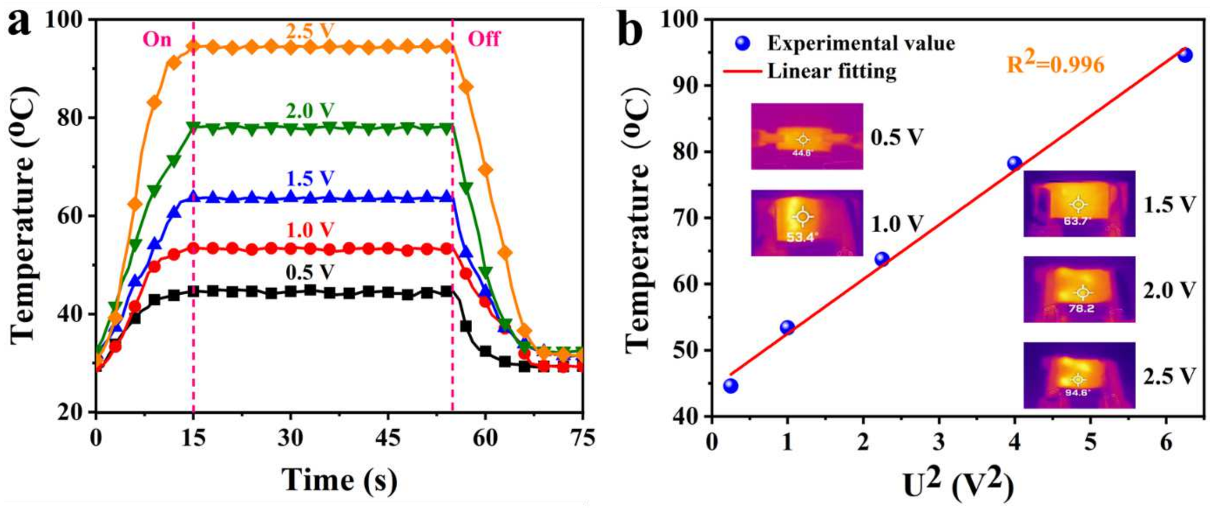

Fig. 7 (a) Temperature variation of MXene-AgNWs/CNT films with time at different operating voltages; (b) Experimental data and linear fitting of saturation temperature versus U^2 and infrared images at different voltages.

4. Conclusion

In summary, we have developed a multifunctional sandwich bionic CNF/Mxene-AgNWs porous film with excellent EMI shielding and Joule heating performance. The sandwich bionic porous films were constructed through vacuum-assisted filtration and freeze-drying method using cellulose nanofibers as the substrate, MXene-AgNWs as the porous internal, revealing high EMI SE (67.5 dB), excellent SSE/t (10675 dB cm^2g^{-1}), enhanced absorption coefficient up to 0.4 at a thickness of only 0.4 mm and excellent mechanical properties with a tensile strength of 20.3 MPa and a fracture strain of 2.1%. In addition, the prepared sandwich bionic MXene-AgNWs/CNF porous films exhibited excellent electrical heating performance and fast temperature response, which ensured the normal function of the prepared composite films under cold condition and facilitated the adaptation to complex application environments. Overall, the sandwich bionic porous films with excellent EMI shielding properties, high mechanical performance, and outstanding electrical heating performance, are potentially applied in the field of high-performance multifunctional EMI shielding materials and thermal management.

Data availability statement

The raw/processed data required to reproduce these findings cannot be shared at this time as the data also forms part of the ongoing study.

Ethics declarations

Conflict of interest

The authors declare that they have no competing interests as defined by Springer, or other interests that might be perceived to influence the results and/or discussion reported in this paper.

Consent for publication

The manuscript is approved by all authors for publication.

Ethical approval and consent to participate

According to the guide for authors, I would like to declare on behalf of my co-author that this work described was an original comment that has not been published previously. All the authors listed have approved the manuscript that is enclosed.

CRediT author statement

Fang Ren: Writing-original draft, Data curation, Software. **Jiale Zhang:** Methodology, Formal analysis, Resources. **Tong Wu:** Validation, Software. **Fudong Zhang:** Data curation, Formal analysis. **Zhengzheng Guo:** Software. **Yanling Jin:** Supervision, Resources. **Penggang Ren:** Conceptualization, Resources.

Acknowledgement

This work was supported by the National Natural Science Foundation of China (Grant No. 52102303), the China Postdoctoral Science Foundation (2019M650268), the Natural Science

Basic Research Program of Shaanxi Province (Grant No. 2022JM-257) and Foundation of Education Department of Shaanxi Province [20JK0805].

References

Abbasi, H., Antunes, M., & Ignacio Velasco, J. (2019). Recent advances in carbon-based polymer nanocomposites for electromagnetic interference shielding. *Progress in Materials Science,* 103, 319-373.

Bai, Y., Bi, S., Wang, W., Ding, N., Lu, Y., Jiang, M., . . . Zhao, Q. (2022). Biocompatible, stretchable, and compressible cellulose/MXene hydrogel for strain sensor and electromagnetic interference shielding. *Soft Materials,* 20(4), 444-454.

Cao, M.-S., Cai, Y.-Z., He, P., Shu, J.-C., Cao, W.-Q., & Yuan, J. (2019). 2D MXenes: Electromagnetic property for microwave absorption and electromagnetic interference shielding. *Chemical Engineering Journal,* 359, 1265-1302.

Cao, W.-T., Chen, F.-F., Zhu, Y.-J., Zhang, Y.-G., Jiang, Y.-Y., Ma, M.-G., & Chen, F. (2018). Binary Strengthening and Toughening of MXene/Cellulose Nanofiber Composite Paper with Nacre-Inspired Structure and Superior Electromagnetic Interference Shielding Properties. *Acs Nano,* 12(5), 4583-4593.

Chen, Q., Zhang, K., Huang, L., Li, Y., & Yuan, Y. (2022). Reduced Graphene Oxide/MXene Composite Foam with Multilayer Structure for Electromagnetic Interference Shielding and Heat Insulation Applications. *Advanced Engineering Materials,* 24(9).

Chen, Z., Xu, C., Ma, C., Ren, W., & Cheng, H.-M. (2013). Lightweight and Flexible Graphene Foam Composites for High-Performance Electromagnetic Interference Shielding.

Advanced Materials, 25(9), 1296-1300.

Cheng, Y., Lu, Y., Xia, M., Piao, L., Liu, Q., Li, M., . . . Wang, D. (2021). Flexible and lightweight MXene/silver nanowire/polyurethane composite foam films for highly efficient electromagnetic interference shielding and photothermal conversion. *Composites Science and Technology,* 215.

Deng, Z., Tang, P., Wu, X., Zhang, H.-B., & Yu, Z.-Z. (2021). Superelastic, Ultralight, and Conductive Ti3C2Tx MXene/Acidified Carbon Nanotube Anisotropic Aerogels for Electromagnetic Interference Shielding. *Acs Applied Materials & Interfaces,* 13(17), 20539-20547.

Fan, Z., Wang, D., Yuan, Y., Wang, Y., Cheng, Z., Liu, Y., & Xie, Z. (2020). A lightweight and conductive MXene/graphene hybrid foam for superior electromagnetic interference shielding. *Chemical Engineering Journal,* 381.

Guo, Z., Ren, P., Lu, Z., Hui, K., Yang, J., Zhang, Z., . . . Ren, F. (2022). Multifunctional $CoFe_2O_4$@MXene-AgNWs/Cellulose Nanofiber Composite Films with Asymmetric Layered Architecture for High-Efficiency Electromagnetic Interference Shielding and Remarkable Thermal Management Capability. *Acs Applied Materials & Interfaces,* 14(36), 41468-41480.

Guo, Z., Ren, P., Wang, J., Hou, X., Tang, J., Liu, Z., . . . Ren, F. (2023). Methylene blue adsorption derived thermal insulating N, S-co -doped TiC/ carbon hybrid aerogel for high-efficient absorption-dominant electromagnetic interference shielding. *Chemical Engineering Journal,* 451.

Guo, Z., Ren, P., Wang, J., Tang, J., Zhang, F., Zong, Z., . . . Ren, F. (2022). Multifunctional sandwich-structured magnetic-electric composite films with Joule heating capacities toward absorption-dominant electromagnetic interference shielding. *Composites Part B-Engineering,* 236.

Han, M., Yin, X., Hantanasirisakul, K., Li, X., Iqbal, A., Hatter, C. B., . . . Gogotsi, Y. (2019). Anisotropic MXene Aerogels with a Mechanically Tunable Ratio of Electromagnetic Wave Reflection to Absorption. *Advanced Optical Materials,* 7(10).

Hu, X., Zhu, C., Quan, B., Sheng, M., Wu, H., Lu, X., & Qu, J. (2022). Engineering robust multifunctional composites with enhanced electromagnetic interference shielding and all-weather thermal management capability via simple layer-by-layer assembly. *Chemical Engineering Journal,* 446.

Iqbal, A., Sambyal, P., & Koo, C. M. (2020). 2D MXenes for Electromagnetic Shielding: A Review. *Advanced Functional Materials,* 30(47).

Iqbal, A., Shahzad, F., Hantanasirisakul, K., Kim, M.-K., Kwon, J., Hong, J., . . . Koo, C. M. (2020). Anomalous absorption of electromagnetic waves by 2D transition metal carbonitride Ti3CNTx (MXene). *Science,* 369(6502), 446-+.

Jia, X., Shen, B., Zhang, L., & Zheng, W. (2021). Construction of shape-memory carbon foam composites for adjustable EMI shielding under self-fixable mechanical deformation. *Chemical Engineering Journal,* 405.

Kim, B. R., Lee, H. K., Kim, E., & Lee, S.-H. (2010). Intrinsic electromagnetic radiation shielding/absorbing characteristics of polyaniline-coated transparent thin films. *Synthetic Metals,* 160(17-18), 1838-1842.

Lapka, T., Vilcakova, J., Kopecky, D., Prokes, J., Dendisova, M., Moucka, R., . . . Hassouna, F.

(2023). Flexible, ultrathin and light films from one-dimensional nanostructures of polypyrrole and cellulose nanofibers for high performance electromagnetic interference shielding. *Carbohydrate Polymers,* 309.

Li, Y., Chen, Y., Liu, Y., Zhang, C., & Qi, H. (2021). Holocellulose nanofibrils assisted exfoliation to prepare MXene-based composite film with excellent electromagnetic interference shielding performance. *Carbohydrate Polymers,* 274.

Li, Y., Shen, B., Pei, X., Zhang, Y., Yi, D., Zhai, W., . . . Zheng, W. (2016). Ultrathin carbon foams for effective electromagnetic interference shielding. *Carbon,* 100, 375-385.

Liu, H., Wang, Z., Wang, J., Yang, Y., Wu, S., You, C., . . . Li, Y. (2022). Structural evolution of MXenes and their composites for electromagnetic interference shielding applications. *Nanoscale,* 14(26), 9218-9247.

Liu, J., McKeon, L., Garcia, J., Pinilla, S., Barwich, S., Mobius, M., . . . Nicolosi, V. (2022). Additive Manufacturing of Ti3C2-MXene-Functionalized Conductive Polymer Hydrogels for Electromagnetic-Interference Shielding. *Advanced Materials,* 34(5).

Liu, J., Zhang, H.-B., Sun, R., Liu, Y., Liu, Z., Zhou, A., & Yu, Z.-Z. (2017). Hydrophobic, Flexible, and Lightweight MXene Foams for High-Performance Electromagnetic-Interference Shielding. *Advanced Materials,* 29(38).

Oliveira, F. M., & Gusmao, R. (2020). Recent Advances in the Electromagnetic Interference Shielding of 2D Materials beyond Graphene. *Acs Applied Electronic Materials,* 2(10), 3048-3071.

Quero, F., & Rosenkranz, A. (2021). Mechanical Performance of Binary and Ternary Hybrid MXene/Nanocellulose Hydro- and Aerogels - A Critical Review. *Advanced Materials*

Interfaces, 8(18).
Shahzad, F., Alhabeb, M., Hatter, C. B., Anasori, B., Hong, S. M., Koo, C. M., & Gogotsi, Y. (2016). Electromagnetic interference shielding with 2D transition metal carbides (MXenes). *Science,* 353(6304), 1137-1140.
Tan, H., Gou, J., Zhang, X., Ding, L., & Wang, H. (2023). Sandwich-structured Ti3C2Tx-MXene/reduced-graphene-oxide composite membranes for high-performance electromagnetic interference and infrared shielding. *Journal of Membrane Science,* 675.
Tang, X., Luo, J., Hu, Z., Lu, S., Liu, X., Li, S., . . . Liu, T. (2022). Ultrathin, flexible, and oxidation-resistant MXene/graphene porous films for efficient electromagnetic interference shielding. *Nano Research*.
Wan, Y., Xiong, P., Liu, J., Feng, F., Xun, X., Gama, F. M., . . . Xu, Y. (2021). Ultrathin, Strong, and Highly Flexible Ti3C2Tx MXene/Bacterial Cellulose Composite Films for High-Performance Electromagnetic Interference Shielding. *Acs Nano,* 15(5), 8439-8449.
Wang, J., Ma, X., Zhou, J., Du, F., & Teng, C. (2022). Bioinspired, High-Strength, and Flexible MXene/Aramid Fiber for Electromagnetic Interference Shielding Papers with Joule Heating Performance. *Acs Nano,* 16(4), 6700-6711.
Wang, L., Shi, X., Zhang, J., Zhang, Y., & Gu, J. (2020). Lightweight and robust rGO/sugarcane derived hybrid carbon foams with outstanding EMI shielding performance. *Journal of Materials Science & Technology,* 52, 119-126.
Wang, Y.-Y., Zhou, Z.-H., Zhou, C.-G., Sun, W.-J., Gao, J.-F., Dai, K., . . . Li, Z.-M. (2020). Lightweight and Robust Carbon Nanotube/Polyimide Foam for Efficient and Heat-Resistant Electromagnetic Interference Shielding and Microwave Absorption. *Acs Applied*

Materials & Interfaces, 12(7), 8704-8712.

Wang, Z., Cheng, Z., Fang, C., Hou, X., & Xie, L. (2020). Recent advances in MXenes composites for electromagnetic interference shielding and microwave absorption. *Composites Part a-Applied Science and Manufacturing,* 136.

Wei, Q., Pei, S., Qian, X., Liu, H., Liu, Z., Zhang, W., . . . Ren, W. (2020). Superhigh Electromagnetic Interference Shielding of Ultrathin Aligned Pristine Graphene Nanosheets Film. *Advanced Materials,* 32(14).

Wu, N., Yang, Y., Wang, C., Wu, Q., Pan, F., Zhang, R., . . . Zeng, Z. (2023). Ultrathin Cellulose Nanofiber Assisted Ambient-Pressure-Dried, Ultralight, Mechanically Robust, Multifunctional MXene Aerogels. *Advanced Materials,* 35(1).

Wu, X., Han, B., Zhang, H.-B., Xie, X., Tu, T., Zhang, Y., . . . Yu, Z.-Z. (2020). Compressible, durable and conductive polydimethylsiloxane-coated MXene foams for high-performance electromagnetic interference shielding. *Chemical Engineering Journal,* 381.

Xu, H., Yin, X., Li, X., Li, M., Liang, S., Zhang, L., & Cheng, L. (2019). Lightweight Ti2CTx MXene/Poly(vinyl alcohol) Composite Foams for Electromagnetic Wave Shielding with Absorption-Dominated Feature. *Acs Applied Materials & Interfaces,* 11(10), 10198-10207.

Yu, Z., Dai, T., Yuan, S., Zou, H., & Liu, P. (2020). Electromagnetic Interference Shielding Performance of Anisotropic Polyimide/Graphene Composite Aerogels. *Acs Applied Materials & Interfaces,* 12(27), 30990-31001.

Yun, T., Kim, H., Iqbal, A., Cho, Y. S., Lee, G. S., Kim, M.-K., . . . Koo, C. M. (2020). Electromagnetic Shielding of Monolayer MXene Assemblies. *Advanced Materials,* 32(9).

Zeng, Z., Jin, H., Chen, M., Li, W., Zhou, L., & Zhang, Z. (2016). Lightweight and Anisotropic

Porous MWCNT/WPU Composites for Ultrahigh Performance Electromagnetic Interference Shielding. *Advanced Functional Materials,* 26(2), 303-310.

Zhai, J., Cui, C., Li, A., Guo, R., Cheng, C., Ren, E., . . . Zhang, J. (2022). Waste cotton Fabric/MXene composite aerogel with heat generation and insulation for efficient electromagnetic interference shielding. *Ceramics International,* 48(10), 13464-13474.

Zhan, Z., Song, Q., Zhou, Z., & Lu, C. (2019). Ultrastrong and conductive MXene/cellulose nanofiber films enhanced by hierarchical nano-architecture and interfacial interaction for flexible electromagnetic interference shielding. *Journal of Materials Chemistry C,* 7(32), 9820-9829.

Zhang, F., Ren, P., Guo, Z., Wang, J., Chen, Z., Zong, Z., . . . Ren, F. (2022). Asymmetric multilayered MXene-AgNWs/cellulose nanofiber composite films with antibacterial properties for high-efficiency electromagnetic interference shielding. *Journal of Materials Science & Technology,* 129, 181-189.

Zhang, H.-B., Yan, Q., Zheng, W.-G., He, Z., & Yu, Z.-Z. (2011). Tough Graphene-Polymer Microcellular Foams for Electromagnetic Interference Shielding. *Acs Applied Materials & Interfaces,* 3(3), 918-924.

Zhang, L., Luo, J., Zhang, S., Yan, J., Huang, X., Wang, L., & Gao, J. (2022). Interface sintering engineered superhydrophobic and durable nanofiber composite for high-performance electromagnetic interference shielding. *Journal of Materials Science & Technology,* 98, 62-71.

Zhang, Y., & Gu, J. (2022). A Perspective for Developing Polymer-Based Electromagnetic Interference Shielding Composites. *Nano-Micro Letters,* 14(1).

Zhang, Y., Ruan, K., & Gu, J. (2021). Flexible Sandwich-Structured Electromagnetic Interference Shielding Nanocomposite Films with Excellent Thermal Conductivities. *Small,* 17(42).

Zhang, Y., Ruan, K., Shi, X., Qiu, H., Pan, Y., Yan, Y., & Gu, J. (2021). Ti3C2Tx/rGO porous composite films with superior electromagnetic interference shielding performances. *Carbon,* 175, 271-280.

Zhu, Y., Liu, J., Guo, T., Wang, J. J., Tang, X., & Nicolosi, V. (2021). Multifunctional Ti3C2Tx MXene Composite Hydrogels with Strain Sensitivity toward Absorption-Dominated Electromagnetic- Interference Shielding. *Acs Nano,* 15(1), 1465-1474.

Zong, Z., Ren, P., Guo, Z., Wang, J., Hu, J., Chen, Z., . . . Ren, F. (2022). Synergistic effect of 2D TiC and 1D CNT towards absorption-dominant high-performance electromagnetic interference shielding in 3D macroporous carbon aerogel. *Carbon,* 197, 40-51.

Supplementary Files

This is a list of supplementary files associated with this preprint. Click to download.

- file.docx